Original Research Article

Harnessing Bankable Wind-Wave Energy Potentials over Offshore Ondo State, Southwestern Nigeria

.

ABSTRACT

Nigeria's power sector faces significant challenges due to generation and distribution inefficiencies, as well as its dependence on hydro energy, making it crucial to tap into the country's renewable energy potential to meet increasing demand. This study evaluated the renewable energy prospects in selected coastal areas of Ondo State, located between latitudes 5.83°N–6.3°N and longitudes 1°E–5.08°E. The research utilized hindcast data of wind and wave parameters, averaged hourly, from January 1, 2012, to December 31, 2024, generated using the Wavewatch III (WW3) model. The model's performance was validated against in-situ buoy measurements. Wind power density was calculated using a two-parameter Weibull distribution function combined with the gamma function. Areas with high wave power density, defined as those with seasonal averages exceeding 6 kW/m and a coefficient of variation (COV) below 2.0, were identified as energy-rich zones. The study also examined and discussed the spatio-temporal variations of wind-wave energy resources, pinpointing locations with abundant clean renewable energy. Results revealed that the highest wave power (>6 kW/m) occurs between longitudes 3.250°E and 3.750°E, making this region most suitable for wave energy exploitation and the development of wave energy converter systems. The maximum wind power density (WPD) values, ranging from 110–120 W/m², were observed in the expansive waters between Seme Kpodji and Ghana, with a mean WPD of 84.83 W/m². These high-energy offshore zones provide a strong foundation for future wind-wave hybrid systems and the sustainable electrification of Nigeria's coastal regions.

Keywords: Renewable energy; Wind power; Wave power; distribution; region; variation.

1. INTRODUCTION

The ocean holds enormous potential for renewable energy generation, making the growth of the ocean energy sector essential for achieving a sustainable future. Looking ahead, harnessing energy from waves, tides, ocean thermal gradients, and floating offshore wind could revolutionize ocean-based energy systems and significantly reduce global dependence on fossil fuels (Tabibi, 2024). The development of ocean energy has a long history, beginning with early experiments in wave and tidal power. Over time, technological progress, driven by scientific research, supportive government policies, and international initiatives, has led to the creation of advanced systems capable of unlocking the ocean's vast energy reserves (Tabibi, 2024). One of the key benefits of ocean energy lies in its environmental advantages over traditional energy sources. Unlike fossil fuels, it is renewable, produces very low greenhouse gas emissions, and leaves a small carbon footprint. These qualities make ocean energy a vital contributor to reducing global emissions and combating climate change. Moreover, the industry offers substantial economic potential

through job creation and sustainable development, supporting both environmental and economic progress (Tabibi, 2024). However, renewable energy productivity is heavily influenced by the cost of capital for energy projects (Yang *et al.,* 2024).

Offshore Renewable Energy (ORE) has gained attention as a promising clean energy source, with growing interest in combining wave energy converters and offshore wind turbines due to their cost-effectiveness (Perez-Collazo *et al.,* 2015). The shift to sustainable energy has driven innovation in hybrid renewable systems, which combine sources like solar, wind, geothermal, and biomass with storage and backup generators, offering a reliable and cost-effective solution to the intermittency of individual renewables (Korovushkin *et al.,* 2025). Achieving a balance between economic, environmental, social, and technical factors is crucial for boosting system performance and resilience, Giedraityte *et al.* (2025). Western Africa, characterized by its abundance of low-intensity wave energy, offers favorable conditions for wave power development. The region's mild and consistent wave climate could benefit the industry, as it reduces the durability challenges often encountered in high-energy wave environments. Using low-capacity converters, wave energy could become a viable renewable option across much of the region. The national energy sectors and the West African Power Pool (WEPP) already have considerable hydropower capacity and high grid flexibility, allowing them to effectively balance fluctuations from wave energy sources. Consequently, the regional conditions appear well-suited for wave energy deployment. Among Western African nations, Senegal and Cabo Verde experience stronger winds and more powerful waves, giving them higher technical potential for wave power. Offshore wind energy is especially promising in Cabo Verde, where it could play a key role in diversifying the island nation's energy mix and stabilizing other intermittent renewable sources. However, due to Western Africa's wide continental shelf separating land from deep, cold ocean waters, opportunities for land-based Ocean Thermal Energy Conversion (OTEC) are limited despite favorable temperature gradients. In the future, as OTEC technology advances, it could unlock substantial offshore energy potential for West African countries with established offshore industries, leveraging expertise from oil and gas operations. Additionally, the region's relatively calm ocean conditions make it more suitable for deep-sea OTEC installations compared to Eastern or Southern Africa. Over time, the feasibility of floating OTEC systems is expected to increase, though current challenges remain in transporting desalinated water, a byproduct, and energy products like liquid hydrogen from offshore facilities to land for consumption or export (African Development Bank Group, 2021).

The coastlines of Africa are exposed to abundant wave energy, with the strongest wave activity occurring along the southern and eastern regions, from Mozambique, southern Madagascar, and Mauritius to Namibia. South Africa, in particular, experiences the most powerful wave conditions. The extensive Somali coastline also shows significant potential, as do the Atlantic coasts of Senegal, Cabo Verde, and Morocco. Other areas in western and northern Africa possess moderate but dependable wave energy resources. Additionally, Central African nations such as São Tomé and Príncipe and the Congo Republic, along with parts of tropical eastern Africa, benefit from consistent ocean swells. The region's generally moderate and low-risk wave climate makes it attractive for developers seeking stable operating conditions (African Development Bank Group, 2021). In a similar effort to evaluate renewable energy potential along the Indian coastline, Upadhyaya *et al.* (2024) utilized the MIKE 21 SW numerical wave model to analyze wind and wave patterns. Their findings indicated that offshore areas near Goa, Karnataka, Kerala, Tamil Nadu, and Andhra Pradesh demonstrated strong potential for harnessing offshore wind energy through wind turbine installations.

Rusu and Onea (2019) presented an in-depth analysis of the potential advantages of combined wind and wave energy projects situated near major islands. Their study revealed

that wind power density varies between 47.1 W/m² near Borneo and 1430 W/m² near Greenland, while wave power ranges from a minimum of 2.28 kW/m near Sulawesi to a maximum of 68.8 kW/m near Tasmania. They also evaluated the levelised cost of energy (LCOE), finding that certain wind power sites already meet the European Union's 2025 target of 0.11 USD/kWh. In contrast, wave energy systems still exhibit relatively high production costs and remain distant from achieving those economic benchmarks. With global efforts intensifying to decarbonize electricity systems and curb climate change, the volume of research exploring pathways to net-zero power grids has expanded significantly. Gonzalez *et al*. (2024) developed a high-resolution spatial model assessing offshore wind and wave energy as separate but potentially co-located technologies within a zero-emission capacity expansion framework for the Western Interconnection, targeting 2050. Their analysis identified cost thresholds for offshore wind and wave energy to achieve economic competitiveness, showing that full deployment of both technologies could reduce total installed capacity by 17% by 2050. They also demonstrated how energy curtailment, generation patterns, and transmission infrastructure evolve with increased offshore renewable integration. It is important to note that reanalysis methodologies used to generate wind field data for wave modeling introduce certain uncertainties. These stem not only from measurement errors but also from changes in data assimilation processes, particularly following the introduction of satellite observations in 1979 (Caires *et al.,* 2004; Sterl, 2004; Chang, 2007). Despite these limitations, hindcast wave models driven by reanalysis wind data have shown strong consistency with buoy observations (Cox & Swail, 2001; Graham & Diaz, 2001; Caires *et al.,* 2004) and have proven valuable in examining large-scale wave patterns and long-term trends across various temporal scales—from short-term synoptic conditions to multi-decadal variations.

Wave model hindcasts offer several benefits compared to buoy observations, including broader spatial coverage and consistent temporal responses to wind forcing, which make them particularly useful for comparing trends across different ocean basins. The maximum energy-carrying wind speed (VmaxE) refers to the wind speed that produces the highest energy output, while the wind energy density (WED) represents the total energy available over time, calculated by multiplying the wind power density (WPD) by the total number of hours in a year. Both of these parameters can be derived using the Weibull distribution parameters (Caires *et al.,* 2004).

The wind speed that carries the maximum energy (Vmax,E) plays a crucial role in estimating wind energy potential (Akdag & Güler, 2010; Keyhani *et al.,* 2010; Hamad *et al.,* 2006). Although this parameter is not directly linked to the total amount of available wind energy, it significantly influences the performance of wind turbine systems, which operate most efficiently when their rated wind speed closely matches Vmax,E. In a study by Bagiorgas *et al.* (2012), 3-hourly wind speed and direction data from seven buoy stations in the Aegean Sea were analyzed to evaluate wind energy potential using the Weibull distribution's shape (k) and scale (c) parameters. The results showed that the highest average wind speed, 7.45 m/s at 10 meters above sea level, occurred at Mykonos, while the lowest values were recorded at Athos (5.08 m/s) and Petrokaravo (5.31 m/s). All other sites exhibited wind speeds exceeding 5.88 m/s. The shape parameter (k) averaged around 1.5 ± 0.25 across all stations, and the scale parameter (c) exceeded 5.89 m/s at most locations, except for Athos, where it measured 4.78 m/s. The maximum energy-carrying wind speed was highest at Mykonos (12.06 m/s) and lowest at Petrokaravo (9.22 m/s). For Athos, the corresponding wind speed that generated peak energy was calculated to be 10.37 m/s, and similar relationships were observed at the other sites.

The abundance of wave energy resources is a key criterion for determining suitable locations for wave power installations (Zheng *et al.,* 2013; Jianli et al., 2008). According to

Osinowo *et al.* (2017), wave energy is considered *available* when wave power equals or exceeds 2 kW/m and *rich* when it reaches or surpasses 20 kW/m. Osinowo *et al.* (2017) analyzed a 37-year, high-resolution reanalysis dataset of 6-hourly wind fields to assess spatial and temporal variations in wind power potential over the mid-Atlantic, using Weibull shape and scale parameters. Their findings showed that wind energy density reached a minimum of 107.5 kWh/m² in September and a maximum of 145.21 kWh/m² in January. The maximum energy-carrying wind speed ranged between 6.59 m/s in October and 6.98 m/s in January. On an annual average basis, the region exhibited a wind power density of 170.23 W/m², a wind energy density of 124.3 kWh/m², a maximum energy-carrying wind speed of 6.81 m/s, and an average wind speed of 5.85 m/s. Based on the wind power classification developed by Elliott and Schwartz (1993) at the Pacific Northwest Laboratory, these values place the mid-Atlantic region in class 3, indicating that it is moderately suitable for wind energy development.

In a recent study, Enikanselu *et al*. (2025) analyzed wind–wave energy distribution across coastal and offshore areas of Ondo State, Nigeria, using daily, one-hourly averaged data on wave height, wave period, and 10 m wind speed from the ERA5 reanalysis dataset, covering the period from January 1, 1989, to December 31, 2023. Their findings revealed that wave power in the range of 0–5 kW/m dominated the region, indicating that the area is generally unsuitable for large-scale wind–wave energy generation. The available energy potential was found to be sufficient only for small-scale, off-grid electrical or mechanical applications. Similarly, Osinowo *et al.* (2018) reported that wave power values between 0 and 10 kW/m were prevalent in the mid-Atlantic. Wind–wave energy production along the offshore zones of Ondo State in southwestern Nigeria depends entirely on the spatial variability of available wind and wave resources. Therefore, before establishing a wind–wave energy farm, it is essential to perform a detailed evaluation of the area's energy potential, followed by more focused assessments in sites showing higher promise (Xydis *et al.,* 2009). Currently, very limited research exists on the wind–wave energy potential in the deeper offshore regions of the Ondo coastline. Building on the work of Enikanselu *et al.* (2025), the present study seeks to extend the investigation further offshore to identify economically viable zones of wind–wave energy concentration. This research analyzes renewable energy characteristics using 13 years (January 1, 2012 – December 31, 2024) of 6-hourly reanalysis data from the European Centre for Medium-Range Weather Forecasts (ECMWF) for wind conditions, along with sea-state hindcast simulations generated by the WAVEWATCH III (WW3) model. The study also aims to locate areas with relatively high wave energy potential that could support the development of wave power plants for electricity generation.

The structure of this paper is as follows: Section 2 describes the study area in detail, while Section 3 outlines the data sources and the methodology employed. Section 4 presents and discusses the results, and Section 5 concludes the study by summarizing the key findings.

2. DESCRIPTION OF THE STUDY AREA

2.1. Geography and Topography of the Study Area

Figure 1 shows the study area, situated between latitudes 5.83°N and 6.3°N and longitudes 1°E and 5.08°E. The water depth gradually increases westward, ranging from 22 m near the Ondo coastal areas to 180 m off the coast of Lome.

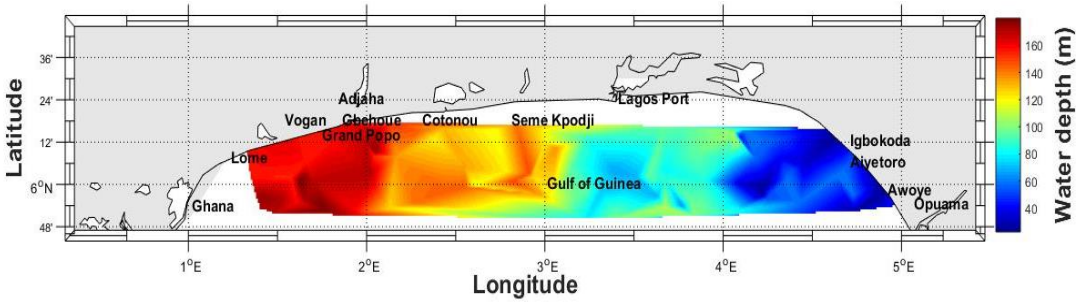

Figure 1. Geography and Topography of the Study Area

The tropical climate of the region features two primary seasons: a rainy season lasting approximately seven months from April to October, and a dry season of about four months from November to March (Osinowo *et al.,* 2024). The coastal areas are typically covered with rainforest vegetation, including dense trees and grasses along riverbanks, and are exposed to high-energy waves that frequently cause the sea to encroach on inhabited areas (Olakunle *et al.,* 2021). The hydrology of the study area is largely influenced by the Niger River, which drains a significant portion of West Africa and delivers sediment-rich water to the Atlantic Ocean through 14 major river outlets (Osinowo & Popoola, 2021). Due to its low-lying, flat terrain, the region is highly susceptible to coastal erosion and flooding, particularly during high tides (Olakunle *et al.,* 2021).

2.2. Rainfall Pattern and Geology of the Study Area

The coastal areas of Ondo State are known for their high rainfall, which varies from about 2,000 mm per year around Irele and Okitipupa to approximately 3,000 mm per year in the Ilaje and Ese-Odo regions (Ishaku & Rafee, 2010). The region's primary shallow hydrogeologic units consist of coastal plain sands, with aquifers typically found in sea sands, continental sands, or gravels. These aquifers are overlain by protective lateritic soils and underlain by the impermeable clay and shale layers of the Akinbo Formation (Omosuyi *et al.,* 2008). The surface geology of the coastal zone is largely composed of the Benin Formation and recent alluvial deposits. Due to the loose and heterogeneous nature of the Benin Formation, the water table is located at considerable depth, often beyond the reach of conventional hand-dug wells (Asiwaju-Bello & Owoseni, 2023).

3. DATA SOURCE AND METHODOLOGY
3.1. Model Description/Data Source

This study utilized WAVEWATCH III (WW3) version 4.18, which features updated source term parameters and improved representation of processes such as wave breaking and dissipation. Bathymetric data from the National Geophysical Data Center's ETOPO 1 were employed to create a high-resolution (0.0170 × 0.0170) water depth grid using Gridgen 3.0. The wind–wave model used default settings for the energy spectra source terms and incorporated the spectrum up to a defined cut-off frequency, with a parametric tail applied beyond it. The model accounted for 36 directional bins and 24 wave numbers, covering frequencies from 0.0412 to 0.4060 Hz and wave periods ranging from 2.4 to 24.7 seconds. The model outputs included two-dimensional wave energy spectra at each grid point on an hourly basis from January 1, 2012, to December 31, 2024. Wind data were sourced from the ERA-Interim reanalysis datasets. The study specifically analyzed model outputs such as 10 m wind speed, significant wave height, mean wave period, mean wave direction, and other wave parameters. Reanalysis combines observational data with numerical models to provide consistent and reliable estimates of atmospheric, wave, and oceanic conditions. The WAM wave model's spectrum was refined using ERA-Interim and satellite altimeter wave height data, though differences between the WW3 and WAM models were observed, reflecting numerical and physical variations.

3.2.1 Data Validation

A comparison was carried out between simulated and observed values of mean wave period, significant wave height, and 10 m wind speed for March and April 2012 to evaluate the reliability of the input data. The resulting correlations are shown in Figure 2.

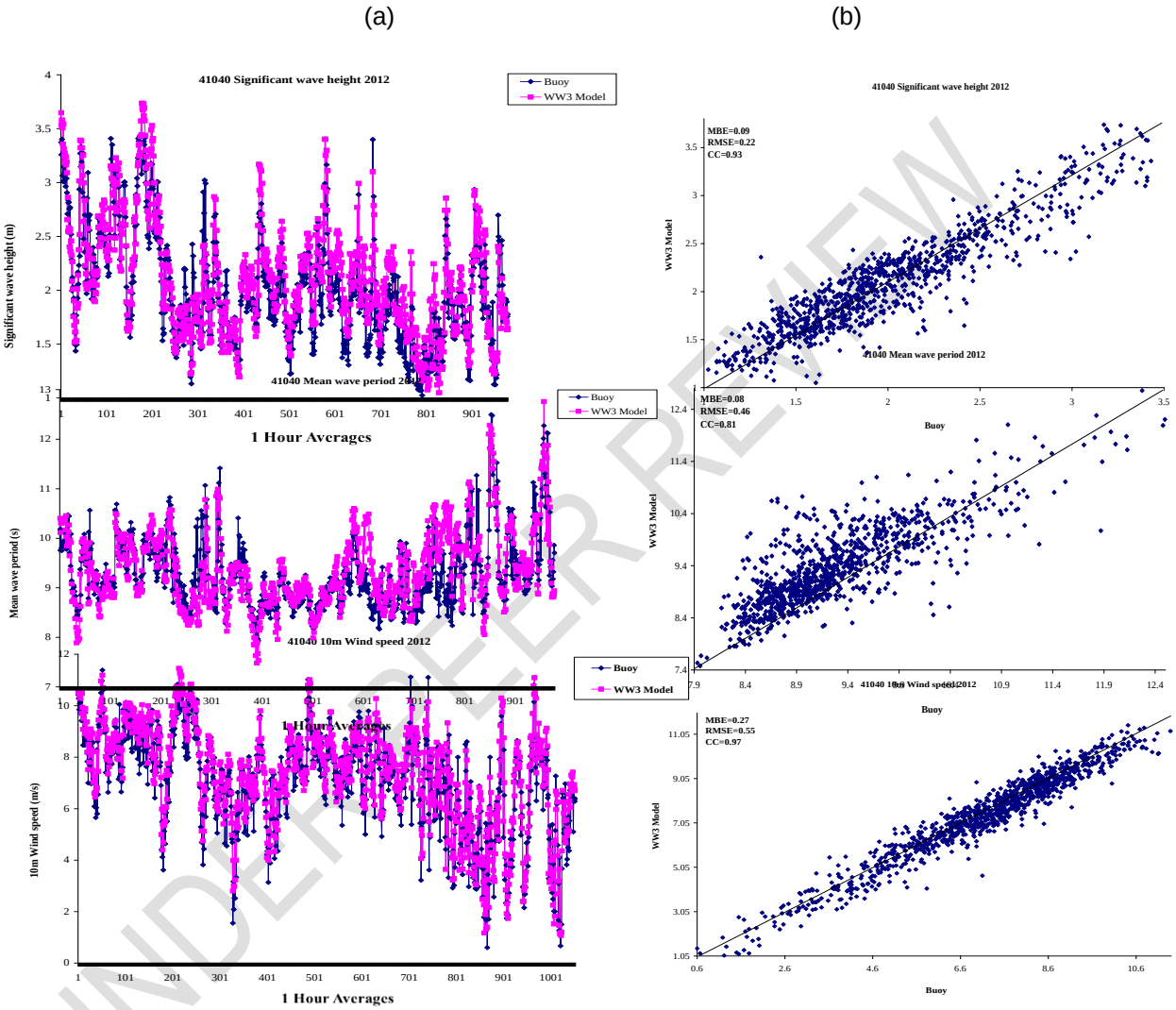

Figure 2. (a) Time Series and (b) Scatter Plots of Model Against Buoy Data for the Significant Wave Heigh from 01-Mar-2012 to 30-Apr-2012t, Mean Wave Period and 10m Wind Speed. On the X-axis is the number of Data Points

Buoy data from the National Data Buoy Center (NDBC) for buoy 41040, located in the North Equatorial One region 470 NM east of Martinique at 14.559° N, 53.073° W (14° 33′ 34″ N, 53° 4′ 23″ W), were used for validation, as it was the nearest station to the study area. Although efforts were made to collect all 1,460 data points for the three variables, gaps in the buoy records, especially for wave parameters, were present. To address these gaps, the model was used to estimate the corresponding wave and wind parameters at the buoy's location. The resulting trends showed strong agreement between the simulated and observed data. The accuracy of the model's wind and wave predictions was evaluated using

standard statistical metrics, including the correlation coefficient, mean bias error, and root mean square error, following the methodology outlined by Wilks (1995).

$$cc = \frac{\sum_{i-1}^{n}(x_i - \bar{x})(y_i - \bar{y})}{\sqrt{\sum_{i-1}^{n}(x_i - \bar{x})^2 \sum_{i-1}^{n}(y_i - \bar{y})^2}} \quad (1)$$

$$Bias = \bar{y} - \bar{x} \quad (2)$$

$$RMSE = \sqrt{\frac{1}{N}\sum_{i-1}^{n}(y_i - x_i)^2} \quad (3)$$

where N is the total number of observations, Xi and Yi stand for the buoy and model data, respectively, and X and Y are the mean values of the two sets of data.

Figure 2 shows a strong agreement between the modeled and observed wave parameters and wind speed, with a correlation coefficient (cc) of 0.8 at the 99% confidence level. The mean bias error (MBE) ranged from 0.08 s to 0.27 m/s, indicating that the buoy measurements were slightly higher than the model predictions. The root mean square error (RMSE) analysis indicated relatively small discrepancies, with errors ranging from 0.22 m to 0.55 s. Overall, the simulation results align well with the observations, suggesting that the reanalysis-driven WW3 wind-wave model provides a more comprehensive and potentially more accurate representation of wind-wave conditions in the study area.

3.3.2 Spatial Data Simulation

The WW3 model used long-term ECMWF ERA-Interim wind field datasets to simulate spatial conditions. The model had a resolution of 0.125° × 0.125° and covered a spatial domain from 20° W to 8.5° E and 20° N to 90° N. Six-hourly zonal (u10) and meridional (v10) wind components were employed, from which the 10 m wind speed was calculated as the square root of the sum of the squares of the u and v components. This generated wind speed outputs at a spatial resolution of 0.1°. The model also produced outputs for mean wave period and significant wave height. The computation domain included both nearshore and offshore regions, spanning 40° N to 70° N and 0° to 60° E, ensuring accurate calculations of wind and wave parameters while minimizing border effects. As illustrated in Figure 1, water-based results were extracted for the study area, which ranges from 5.080° E to 10° E and 5.830° N to 6.30° N. Model outputs were generated at 1-hour intervals, with computational time steps of 360, 180, and 60 seconds. The simulation period extended from January 1, 2012, 00:00, to December 31, 2024, 18:00.

3.3.3 Analysis Methods
3.3.3.1 Computation of Wind Energy

The Weibull probability distribution function is commonly recommended for analyzing wind data because it closely aligns with experimental observations (Ohunakin *et al.,* 2011). This distribution uses a gamma function to estimate wind power density and depict wind speed frequency distributions, making it a useful tool for wind analysis (Gökçek *et al.,* 2007). Historically, several distributions—including Rayleigh, Weibull, log-normal, and normal—have been applied in wind data studies (Fyrippis *et al.,* 2010). Among these, the Weibull

probability density function offers a robust mathematical approach for characterizing wind power density and wind speed distributions (Gökçek *et al.,* 2007), as shown below:

$$f(v) = \frac{k}{c}\left(\frac{v}{c}\right)^{k-1} \exp\left[-\left(\frac{v}{c}\right)^{k}\right] \quad (4)$$

The corresponding cumulative density function is expressed in (Gökçek *et al.,* 2007) as:

$$\mathrm{F}(v) = 1 - \exp\left[-\left(\frac{v}{c}\right)^{k}\right] \quad . \quad (5)$$

Wind speed is represented by "v," while the shape and scale parameters are denoted by "k" and "c," respectively. Wind potential, expressed in meters per second (m/s), can be determined using several techniques, including the standard deviation method (Justus *et al*., 1978), power density approach (Akdag and Dinler, 2009), maximum likelihood estimation (Stevens and Smulders, 1979), and graphical methods (Rinne, 2010). The dimensionless parameter "k" indicates the variability of mean wind speeds within a dataset, where higher "k" values correspond to more consistent winds, and higher "c" values indicate a broader distribution of wind power (Khan *et al.,* 2015). In this study, the wind potential was calculated using the standard deviation method, following the approach of Justus *et al.* (1978) and Saleh *et al.* (2012).

$$k = -\left(\frac{\sigma}{\bar{v}}\right)^{-1.086} \quad \text{for } 1 \le k \le 10 \quad (6)$$

$$c = \frac{\bar{v}}{\Gamma\left(1+1/k\right)} \quad (7)$$

where σ is the standard deviation that describes the degree of wind speed variance, and v is the mean wind speed (m/s). The gamma function, Γ(x), is written as follows in (Manwell *et al.,* 2002):

$$\Gamma(x) = \int_0^{\infty} \exp(-u)u^{x-1}dx \quad (8)$$

Wind power density is expressed in (Sathyajith, 2006) as:

$$Pd = \frac{P(v)}{A} = \frac{1}{2}\rho\int_0^{\infty} v^3 f(v)dv = \frac{1}{2}\rho c^3\Gamma\left(1+\frac{3}{k}\right) \quad (9)$$

where A (w/m^2) is the swept area of the wind turbine rotor, P_d (w/m^2) is the wind power density, P (v) is the wind power in watts, and ρ is the air density, which is taken to be 1.225 kg/m^3.

The wind energy density is expressed in (Tchinda *et al.,* 2000) as:

$$E_d = \frac{1}{2}\rho c^3\Gamma\left(1+\frac{3}{k}\right)T \quad (10)$$

where T is the number of days in the month considered.

The maximum energy carrying wind speed is expressed in (Jamil *et al.,* 1995) as:

$$V_{\max,E} = c\left(1+\frac{2}{k}\right)^{1/k} \quad (11)$$

Wind speed variability is explained by the coefficient of variation (cov), which is the ratio of mean wind speed to mean standard deviation. Ahmed (2012) presented COV in percentage, as stated below:

$$COV\,(\%) = \frac{\sigma}{\bar{V}} \times 100 \tag{12}$$

3.3.3.2 Computation of Wave Energy

The Wave Power Density (WPD) estimation method, as outlined by Cornett (2008), Iglesias and Carballo (2011), and Vosough (2011), was utilized to compute wave energy. It is estimated as follows:

$$P_w = \frac{\rho g^2}{64\Pi} H^2_{mo} T_e = 0.49 H^2_{mo} T_e \tag{13}$$

where P_w represents wave power (unit: kW/m), H_{mo} is the significant wave height (unit: m), and T_e is the mean wave period (unit: s).

A relatively rich energy distribution was identified for Wave Power Density (WPD). According to Zheng et al., (2014), areas with a seasonal average WPD exceeding 6 kW/m and a coefficient of variation (COV) below 2.0 are considered rich energy regions (RER). This concept was applied in this study. Wave power variability can be evaluated using multiple metrics, with the COV being a particularly intuitive one. To assess wave power stability, the COV was calculated for each grid point, revealing that stability increases as the COV decreases.

The COV can be calculated using the following formula:

$$COV = \frac{s}{\bar{x}} \tag{14}$$

where s is the STD and is evaluated as:

$$S = \sqrt{\frac{\sum_{i=1}^{n} x_i^2 - \left(\sum_{i=1}^{n} x_i\right)^2 / n}{n-1}} \tag{15}$$

where $\bar{x}$ is the mean value

The monthly variability index (MVI) is expressed as:

$$MVI = \left(P_M 1 - P_M 12\right) / Pyear \tag{16}$$

where P_M1 and P_M12 are respectively the maximum and minimum monthly mean WVPD, and Pyear is the annual mean WVPD. Higher index values indicate larger wave energy variations, and decreased stability compared with lower index values.

The annual and monthly WVPD was computed using Equation 17. It is expressed as a percentage cumulative frequency, as stated below:

$$f\,(WVPD) = 100\left(n / N\right) \tag{17}$$

where N is the total of the WVPD values, and n is the frequency of WVPD that satisfies each of the stated intervals of WVPD, with respect to various wave powers.

This study examined the bivariate distribution of wave occurrence and total wave power within the study area, analyzing wave height and period at intervals of 2.5 m and 2.5 s. A statistical evaluation of wind-wave data from 2012 to 2024 was performed to investigate wind speed frequency distributions for wind power assessment. Monthly calculations were made for wind power density, wind energy density, maximum energy-carrying wind speed, mean wind speed, standard deviation, coefficient of variation, and Weibull parameters. The spatiotemporal patterns of these parameters were also characterized. Additionally, monthly

ratios of wind speed and wind power density were determined, alongside the spatial distribution of wave power density, wave categories, wave power relative energy ratio (RER), and variability. Temporal changes in wave power density and the monthly variability index were further analyzed.

4. RESULTS AND DISCUSSION

Figure 3 illustrates the direction of ocean surface waves in the study area, revealing a dominant northeasterly orientation. This suggests that the primary waves reaching the region come from the northeast, reflecting a prevailing wind or ocean current from that direction. The northeasterly wave pattern could have important effects on coastal erosion, sediment movement, and maritime operations in the area.

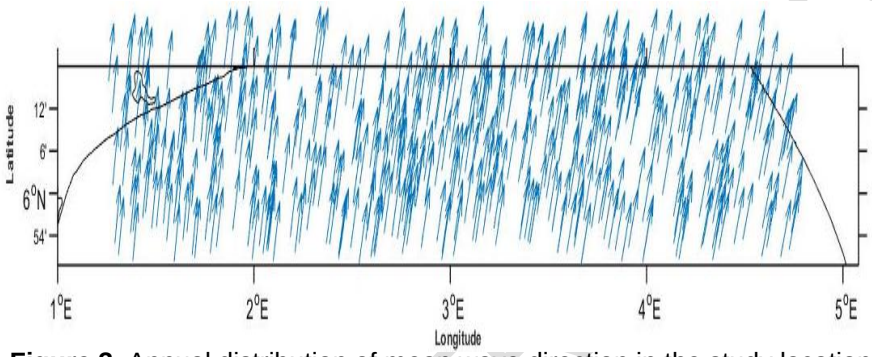

Figure 3. Annual distribution of mean wave direction in the study location.

4.1 Spatio-temporal characteristics of WVPD and wave power RER.

This section analyzed the spatial distribution and temporal trends of Wave Power Density (WVPD) in the study area, emphasizing regional differences in wave energy potential. As shown in Figure 4a, the area generally experienced annual average wave power between 5.2 and 6.4 kW/m. Lower values (<5.6 kW/m) were observed in some eastern regions and near the coasts of Ghana and Lome, while higher values (>6.4 kW/m) were concentrated in waters between 3.250° E and 3.750° E longitudes. Figure 4b depicted the long-term temporal variations of annual mean wave power, indicating a decreasing trend of -0.043 kW/m per year. The lowest annual mean, 5.25 kW/m, occurred in 2021, whereas the highest values were recorded in 2016 and 2017. This overall decline was linked to limited influences from storm activity, atmospheric circulation, and monsoonal variability. Additionally, the pronounced fluctuations in wave power from 2017 to 2022 were associated with hurricane intensity and storm events in the basin, driven by changes in the strength of the West African Monsoon.

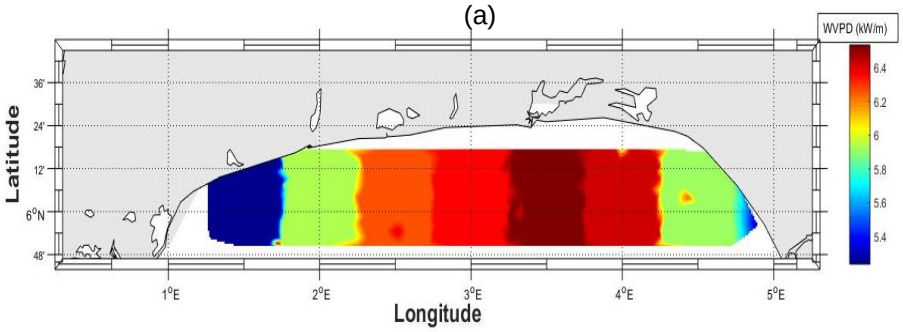

(b)

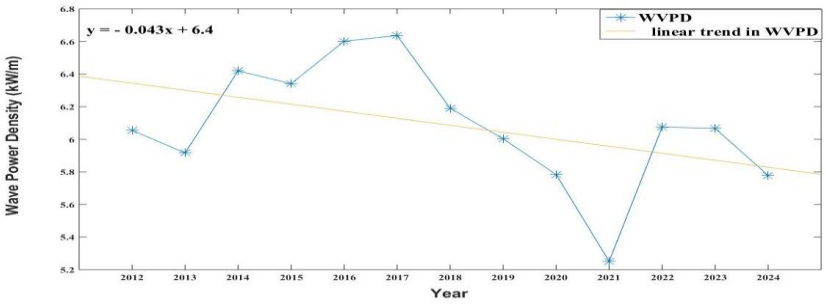

Figure 4. (a) The Spatial and (b) Temporal Variations of the Annual Mean WVPD in the Study Location. Units are in kW/m and kW/myr^{-1} respectively.

4.1.1 Relative rich energy regions of wave power

The study assessed regional variations in wave power density across the area. As shown in Figure 5, the eastern and western portions exhibited relatively low wave power, below 2 kW/m, indicating limited potential for large-scale wave energy generation. This low wave energy was attributed to weak wind speeds, which minimally influence wave conditions. In contrast, waters between 3.250° E and 3.750° E showed the highest wave power, exceeding 6 kW/m, highlighting this zone as the most suitable for deploying wave energy converters for large-scale electricity production. Additionally, a smaller area near the Ondo State coastline, at 4.30° E and 6.10° N, was identified as having relatively high wave power, with energy density around 5 kW/m.

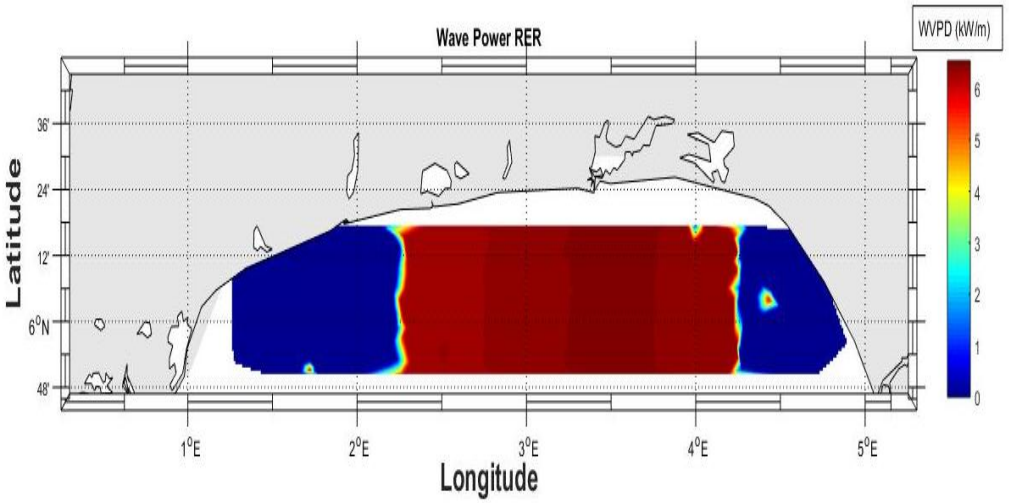

Figure 5. Wave Power in Relative Rich-Energy Regions.

4.2 Spatial Variation of Wave Power for Different Categories

The overall regional distribution of the percentage frequencies of wave power, representative of different categories, is shown in Figure 6.

(a)

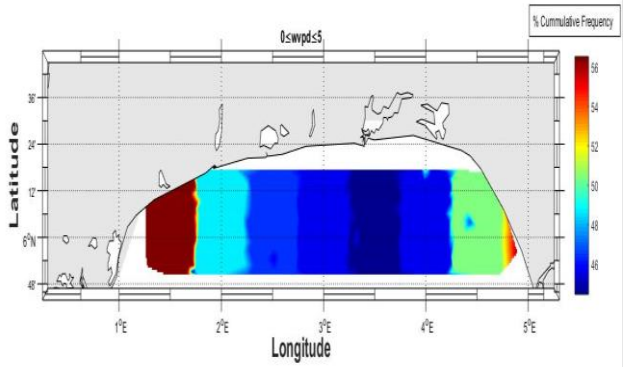
0≤wvpd≤5
% Cummulative Frequency
Latitude
Longitude

(b)

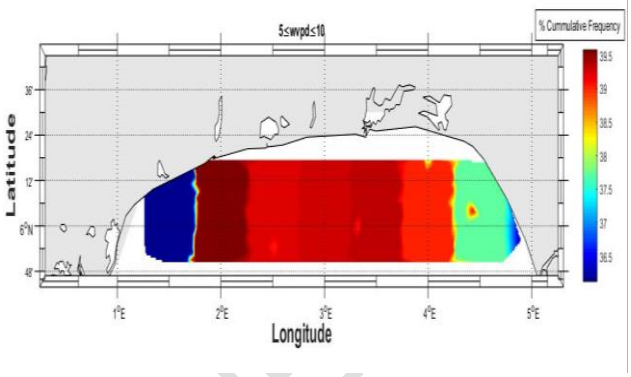
5≤wvpd≤10
% Cummulative Frequency
Latitude
Longitude

(c)

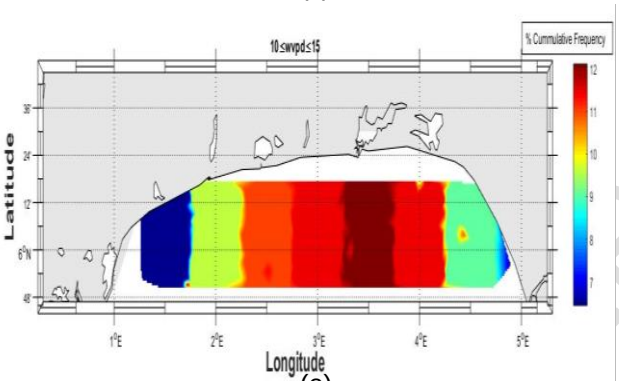
10≤wvpd≤15
% Cummulative Frequency
Latitude
Longitude

(d)

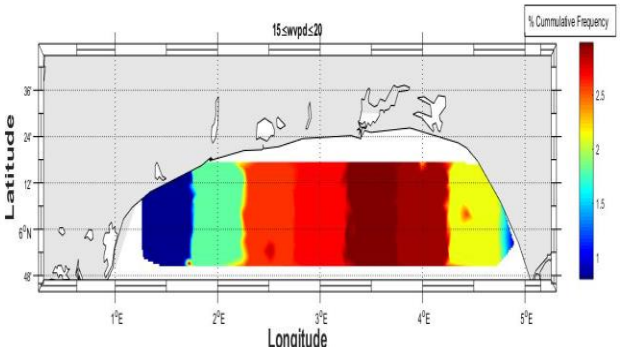
15≤wvpd≤20
% Cummulative Frequency
Latitude
Lonaitude

(e)

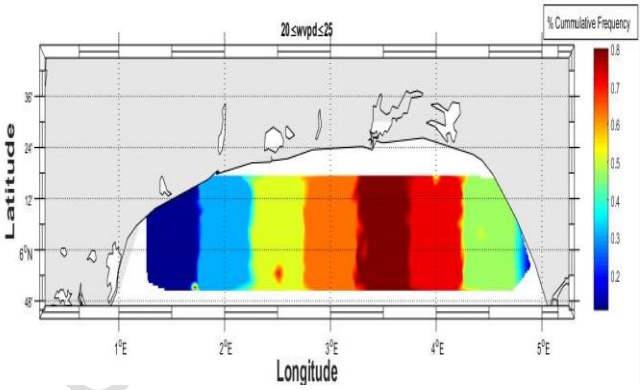
20≤wvpd≤25
% Cummulative Frequency
Latitude
Longitude

(f)

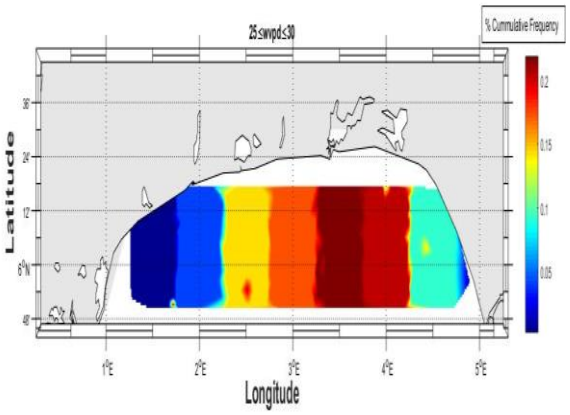
25≤wvpd≤30
% Cummulative Frequency
Latitude
Longitude

(g)

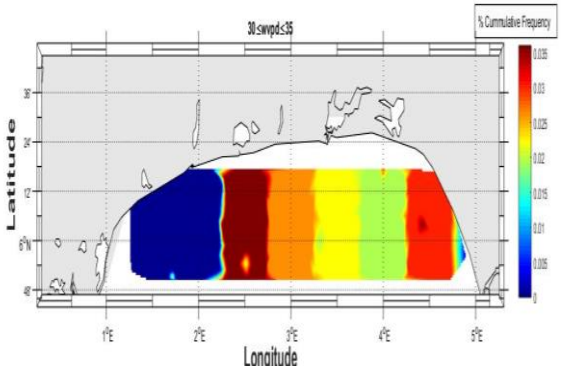
30≤wvpd≤35
% Cummulative Frequency
Latitude
Lonaitude

(h)

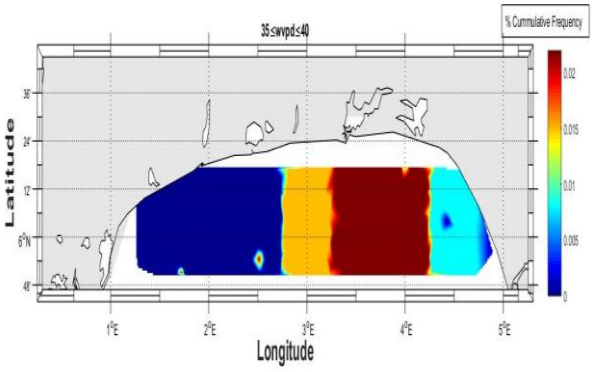
35≤wvpd≤40
% Cummulative Frequency
Latitude
Longitude

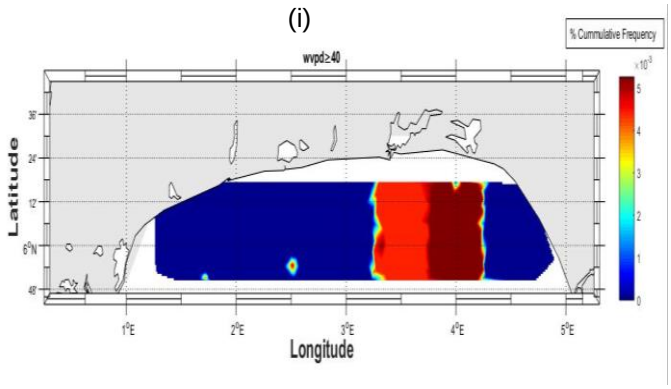

Figures 6 (a-i). Spatial distributions of the percentage cumulative frequencies of *WVPD* for different categories.

Figure 6a shows that the highest percentage frequency of wave power in the 0≤WVPD≤5 kW/m category, approximately 56%, occurred near the coasts of Ghana and Lome, while it was lowest (<46%) in waters between 3.250° E and 3.750° E. Elevated frequencies of around 54% were also observed along the Aiyetoro and Awoye coasts. In the 5≤WVPD≤10 kW/m category (Figure 6b), the highest frequency, about 39.5%, was recorded in waters south of Gbehoue. The frequency increased moving westward toward 3.250° E longitude and decreased south of Seme Kpodji, with the lowest values (<37%) found near Aiyetoro, Awoye, Ghana, Lome, and south of Vogan and Grand Popo. For the 10≤WVPD≤15 kW/m category (Figure 6c), the highest occurrence (~12%) was located between 3.250° E and 3.750° E, while the lowest (<8%) appeared near Aiyetoro, Awoye, and the far western parts of the study area. Wave power exceeding 15 kW/m was rare or absent (<3%) across the entire region.

Table 1 presented the percentage cumulative frequency of annual and monthly wave power density (WVPD) in the study area, calculated using Equation 17. It illustrated the distribution of wave power, ranging from 0 to 40 kW/m, on both an annual and monthly basis.

Table 1. Annual and Monthly Mean Wave Power Percentage Frequencies (*f* is computed using Equation 17)

	0≤wvpd≤5	**5≤wvpd≤10**	**10≤wvpd≤15**	**15≤wvpd≤20**	**20≤wvpd≤25**	**25≤wvpd≤30**	**30≤wvpd≤35**	**35≤wvpd≤40**	**wvpd≥40**
Annual	48.38	38.59	10.12	2.26	0.50	0.12	0.02	0.01	0.00
Jan	84.39	14.68	0.93	0.00	0.00	0.00	0.00	0.00	0.00
Feb	73.31	22.92	2.84	0.91	0.03	0.00	0.00	0.00	0.00
Mar	44.34	33.26	3.48	0.58	0.02	0.00	0.00	0.00	0.00
Apr	46.15	49.61	4.24	0.00	0.00	0.00	0.00	0.00	0.00
May	36.15	53.38	9.18	1.13	0.17	0.00	0.00	0.00	0.00
Jun	18.04	55.29	22.50	3.48	0.66	0.04	0.00	0.00	0.00
Jul	13.09	45.83	28.80	9.11	2.47	0.69	0.00	0.00	0.00
Aug	14.40	51.10	24.45	7.22	1.93	0.56	0.21	0.11	0.02
Sep	23.26	58.30	14.13	3.45	0.65	0.19	0.00	0.00	0.00
Oct	58.22	35.87	5.23	0.65	0.03	0.00	0.00	0.00	0.00

Nov	70.67	25.34	3.64	0.35	0.00	0.00	0.00	0.00	0.00
Dec	88.99	10.58	0.43	0.00	0.00	0.00	0.00	0.00	0.00

The data indicated that wave power values predominantly fell within the 0 to 10 kW/m range throughout the area. Specifically, wave power between 0 and 5 kW/m occurred most frequently from October to March, with frequencies of 58.22%, 70.67%, 88.99%, 84.39%, 73.31%, and 44.34%, respectively. From April to September, higher frequencies were observed in the 5 to 10 kW/m category, recording 49.61%, 53.38%, 55.29%, 45.83%, 51.10%, and 58.30%. Examination of the 10 to 25 kW/m category showed that the sea was most energetic and turbulent between June and August, as reflected by the higher occurrence rates in these months. Minimal or negligible occurrences were noted for the higher wave power categories.

4.3 Wave Power Stability and Bivariate Distribution of Wave Energy.

The pattern of wave power stability in the study area, as indicated by the monthly variability index (MVI), is shown in Figure 7.

(a)

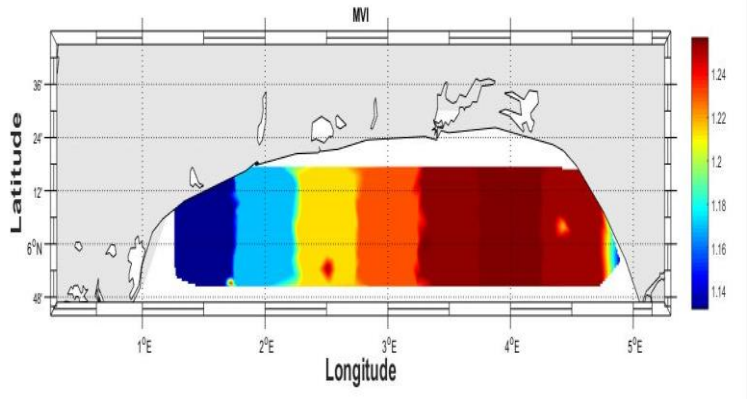

(b)

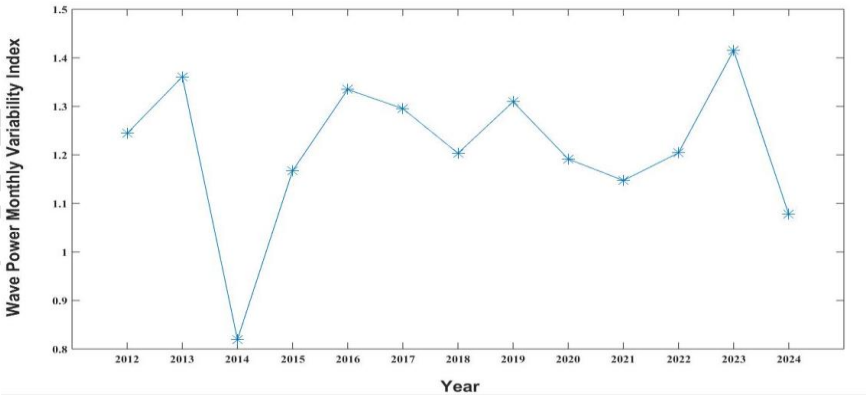

Figure 7. (a) Spatial and (b) Temporal Variation of Wave Power MVI in the Study Area.

As shown in Figure 7a, high MVI (>1.24) regions lie between longitudes 3.3^0 E and 4.7^0 E and in a small region around 5.85^0 N, 2.5^0 E of the study area. These are regions of the lowest stability of wave power. The wave power is most stable (MVI<1.17) around Aiyetoro, Awoye, Ghana, Lome and regions south of Vogan and Grand Popo. For the variability index

presented in Figure 7b, wave power is most stable in the year 2014, with a value of 0.82, and least stable in the year 2023, with value of 1.42.

Table 2 showed a bivariate distribution of wave height (Hs) and wave period (Te) in the study location. It could be seen from the table that the most frequent sea states (bold and highlighted in green) concentrated between 3.5 s and 8.5 s for Te and values ≤ 5 m for Hs.

Table 2. Number of Occurrences of Different Sea States in the Study Area

Hs/Te	1-3.5	3.5-6	6-8.5	>=8.5
0-2.5	3373767	**49855487**	**46484384**	1019908
2.5-5	0	**7491**	**13747**	0

A scatter table is frequently used to display the frequency of occurrence of sea states defined by a characteristic wave height (Hs) and wave period (Te) (Iglesias and Carballo, 2011). The total annual wave power for different sea states is presented in Table 3. It could be seen that the main wave energy (bold and highlighted in green) is also concentrated between 3.5 s and 8.5 s (Te) and for values ≤ 5 m (Hs). When relating these results to the number of occurrences (Table 2), it was observed that the most frequent sea states coincided with the most energetic sea states.

Table 3. Total Wave Power (in GW/m) Corresponding to sea States for Different Ranges of Hs and Te in the Study Area

Hs/Te	1-3.5	3.5-6	6-8.5	>=8.5
0-2.5	9.87	**207.75**	**382.04**	12.90
2.5-5	0.00	**0.14**	**0.50**	0.00

4.4. Wind Characteristics.

The monthly variation of wind and their annual mean values are presented in Table 4.

Table 4. Monthly and Annual Mean Wind Characteristics.

Month	K	c (m/s)	WPD (w/m^2)	u10 (m/s)	σ (m/s)	cov (%)	WPD Ratio (w/m^2)	u10 ratio (m/s)	VmaxE (m/s)	WED (kWh/m^2)
Jan	3.50	4.73	65.30	4.26	1.41	33.33	0.77	0.92	5.44	48.58
Feb	3.81	5.14	81.16	4.64	1.41	30.58	0.96	1.00	5.78	55.08
Mar	4.18	5.35	90.87	4.86	1.38	28.50	1.07	1.05	5.92	67.61
Apr	4.19	4.94	72.18	4.49	1.28	28.81	0.85	0.97	5.46	51.97
May	3.55	4.41	52.81	3.97	1.27	32.50	0.62	0.86	5.02	39.29
Jun	3.82	5.03	78.23	4.55	1.41	31.36	0.92	0.98	5.64	56.32
Jul	6.49	6.61	165.44	6.16	1.19	19.64	1.95	1.33	6.92	123.09
Aug	7.01	6.55	159.73	6.12	1.12	18.49	1.88	1.32	6.83	118.84
Sep	5.19	5.81	114.83	5.35	1.30	24.66	1.35	1.15	6.23	82.68
Oct	3.70	4.52	57.74	4.08	1.33	32.95	0.68	0.88	5.13	42.96
Nov	3.18	3.80	35.21	3.41	1.23	36.23	0.41	0.74	4.46	25.35
Dec	3.21	4.13	44.52	3.70	1.32	35.68	0.52	0.80	4.85	33.12
Annual	4.32	5.09	84.83	4.63	1.30	29.40			5.64	62.07

The shape parameter “k” ranged from 3.18 in November to 7.01 in August, indicating that wind conditions were most stable in August and least stable in November. Therefore, August was identified as the most favorable month for generating continuous and steady wind power. The scale parameter “c” varied between 3.80 m/s in November and 6.61 m/s in July, suggesting that wind speeds were most dispersed in July and least dispersed in November. Monthly mean wind speeds at 10 meters height (u10) ranged from 3.41 m/s in November to 6.16 m/s in July. Wind power density (WPD) fluctuated between 35.21 W/m² in November and 165.44 W/m² in August. The wind speed variation was highest at 1.41 m/s in January, February, and June, and lowest at 1.12 m/s in August. Wind stability, measured by the coefficient of variation (COV), was highest in August (18.49%) and lowest in November (36.23%). The lowest wind energy density (WED) of 25.35 kWh/m² occurred in November, while the highest value of 123.09 kWh/m² was observed in July. Similarly, maximum wind speeds (VmaxE) ranged from 4.46 m/s in November to 6.92 m/s in July. The annual mean WPD and u10 were 84.83 W/m² and 4.63 m/s, respectively. Based on the wind power classification of Elliott and Schwartz (1993) from the Pacific Northwest Laboratory (Table 5), the study area’s annual mean WPD of 84.83 W/m² falls under Class 1, indicating that the region is poor and unsuitable for large-scale wind power generation. However, the wind resources could still support small-scale or off-grid applications, including wind generators, battery charging, water pumping, and agricultural uses. Figure 8a illustrates the monthly variations in WPD and u10 ratios, while Figure 8b shows the percentage frequency distribution of u10 in the area. Both WPD and u10 ratios were highest in July (1.95 W/m² and 1.33 m/s, respectively) and lowest in November (0.41 W/m² and 0.74 m/s, respectively). Wind speeds between 4 and 8 m/s occurred most frequently, with a frequency of 62.63%, followed by speeds of 0 to 4 m/s at 35.51%. Speeds between 8 and 12 m/s were rare, occurring only 1.86% of the time, while speeds above 12 m/s were not recorded.

Table 5. Wind power classification (Enikanselu *et al.,* 2025).

Power Class	Power density (w/m²) at 10m	Resource Potential
1	0 < P ≤ 100	Not Suitable
2	100 < P ≤ 150	Marginal
3	150 < P ≤ 200	Fair
4	200 < P ≤ 250	Good
5	250 < P ≤ 300	Excellent
6	300 < P ≤ 400	Outstanding
7	400 < P ≤ 1000	Superb

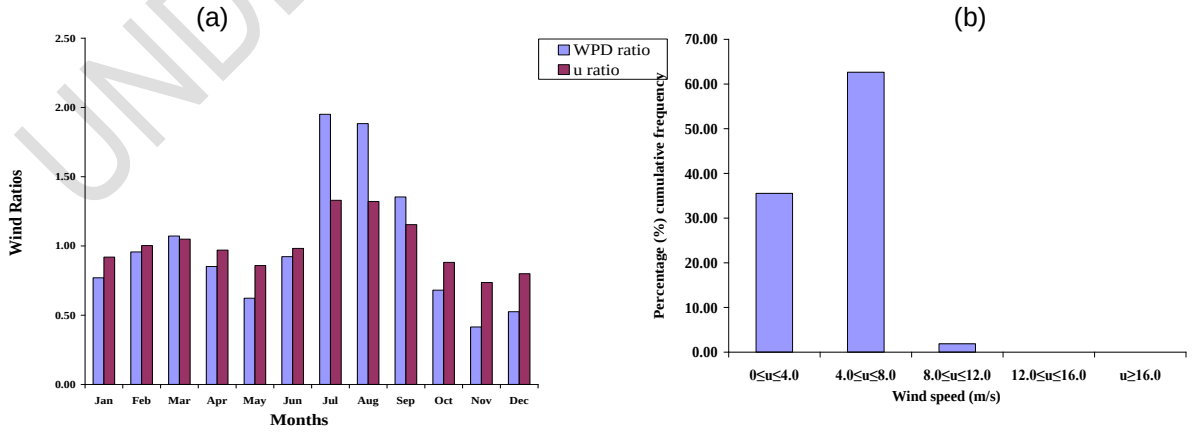

Figure 8. (a) Monthly Variation in the Wind Ratios and (b) Percentage frequency distribution of wind speed in the study area.

4.4.1 Spatio-Temporal Variation of Wind Parameters.

The spatial distribution of wind parameters—including “k,” “c” (m/s), WPD (m/s), u10 (m/s), σ, COV (%), VmaxE (m/s), and WED (kWh/m²)—is illustrated in Figures 9(a–h). The “k” values in Figure 9a, ranging from 2.53 along the coasts of Igbokoda, Aiyetoro, and Awoye to 3.85 in areas south of Lome, indicate that wind stability tends to increase toward the west. Figure 9b shows the “c” values, which are highest (5.53–5.87 m/s) across a wide area between Seme Kpodji and Ghana, suggesting that wind power is more broadly distributed in the western part of the study area. The distributions of WPD, u10, VmaxE, and WED (Figures 9c, d, g, and h) follow a similar pattern to “c,” with higher values concentrated over the waters between Seme Kpodji and Ghana and lower values along the coasts of Igbokoda, Aiyetoro, Awoye, and Opuama. The WPD in Figure 9c classifies regions immediately south of Cotonou and near Ghana as Class 2, indicating marginal potential for grid-connected wind power. Most of the study area falls under Class 1 (WPD < 100 W/m²), which is suitable only for small-scale turbines due to low energy potential. Figures 9e and 9f display wind speed variability (σ) and the coefficient of variation (COV), respectively. Higher σ values correspond to greater fluctuations in wind speed. The central part of the study region exhibits the highest variability (1.65 ≤ σ ≤ 1.7), whereas the coast of Awoye has the most stable winds (σ ≤ 1.25). Consistent with the “k” parameter, the wind speed COV in Figure 9f shows increasing wind stability toward the west, ranging from 42.4% to 28.9%.

Long-term trends in the annual average values of the wind parameters, analyzed through linear regression with a 95% confidence level, are shown in Figures 10(a–d). These trends were based on the regional mean wind energy calculated from 00:00 UTC on January 1, 2012, to 18:00 UTC on December 31, 2024. In Figure 10a, the regression coefficients for VmaxE and u10 were 0.01 and 0.0003, indicating that VmaxE and u10 increased at rates of 0.01 m/s per year and 0.0003 m/s per year, respectively. The u10 reached its minimum (4.44 m/s) in 2016 and maximum (4.78 m/s) in 2018, while VmaxE was lowest (5.42 m/s) in 2012 and highest (5.83 m/s) in 2022. For the “k” and “c” parameters (Figure 10b), the regression coefficients were -0.016 and 0.005, showing a decrease in “k” of 0.016 per year and an increase in “c” of 0.005 m/s per year. “k” was lowest (3.61) in 2017 and highest (4.35) in 2013, while “c” ranged from 4.72 m/s in 2012 to 5.19 m/s in 2018. Figure 10c presents WPD and WED trends, with regression coefficients of 0.29 and 2.6, indicating annual increases of 0.29 W/m² and 2.6 kWh/m² per year, respectively. The WPD was lowest (74.02 W/m²) in 2016 and highest (92.57 W/m²) in 2022, while WED followed the same pattern, ranging from 650.16 kWh/m² to 810.9 kWh/m². Finally, Figure 10d shows the trends for wind speed σ and wind speed COV, with regression coefficients of 0.01 and 0.21, suggesting that σ increased by 0.01 m/s per year and COV by 0.21% per year. The σ values were lowest (1.41 m/s) in 2013 and highest (1.66 m/s) in 2019, while COV ranged from 30.23% to 36.22% during the same years.

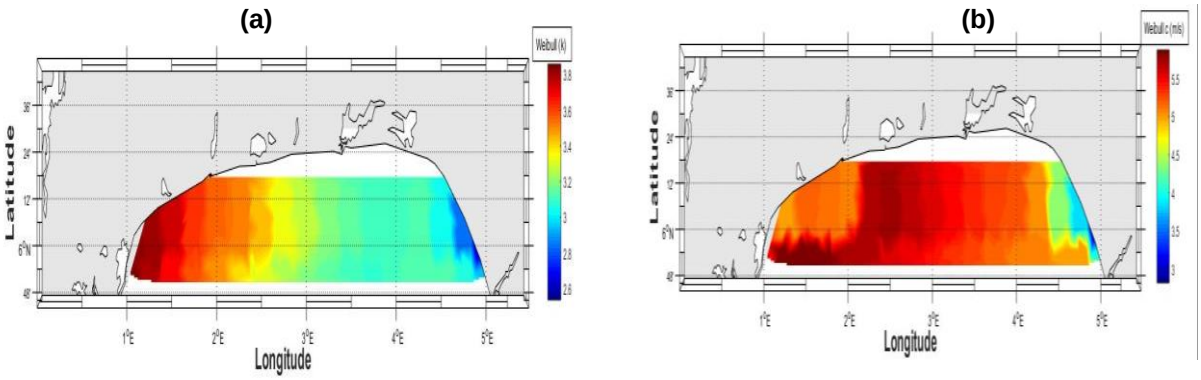

(c)

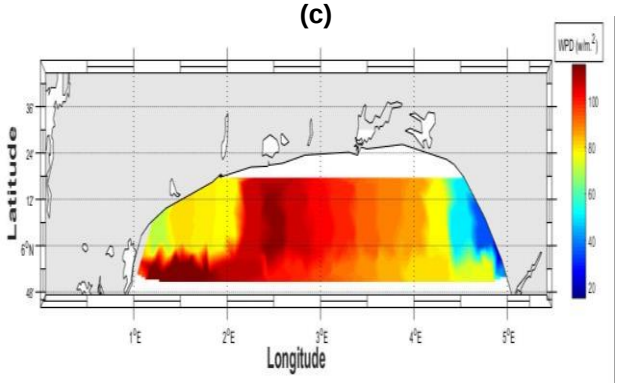
WPD (w/m^2)
100
80
60
40
20
Latitude
36
24
12
6°N
48
1°E
2°E
3°E
4°E
5°E
Longitude

(d)

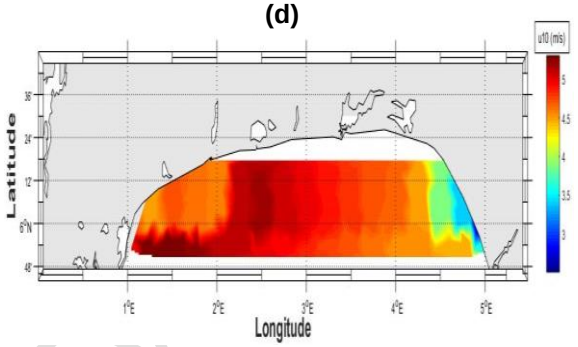
u10 (m/s)
5
4.5
4
3.5
3
Latitude
36
24
12
6°N
48
1°E
2°E
3°E
4°E
5°E
Longitude

(e)

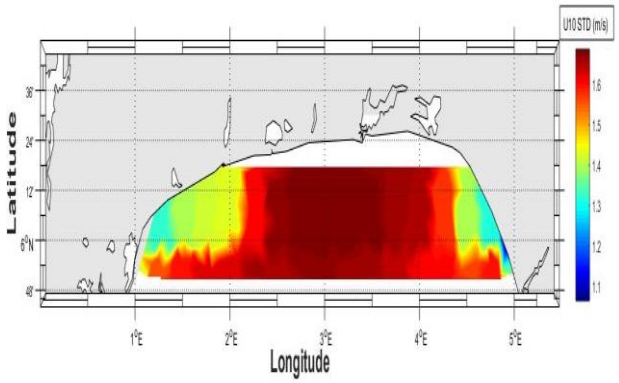
U10 STD (m/s)
1.6
1.5
1.4
1.3
1.2
1.1
Latitude
36
24
12
6°N
48
1°E
2°E
3°E
4°E
5°E
Longitude

(f)

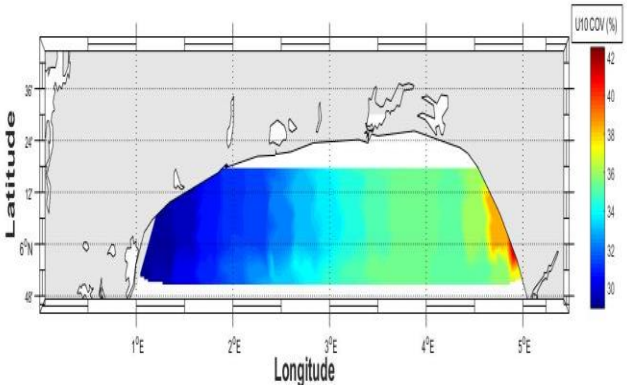
U10 COV (%)
42
40
38
36
34
32
30
Latitude
36
24
12
6°N
48
1°E
2°E
3°E
4°E
5°E
Longitude

(g)

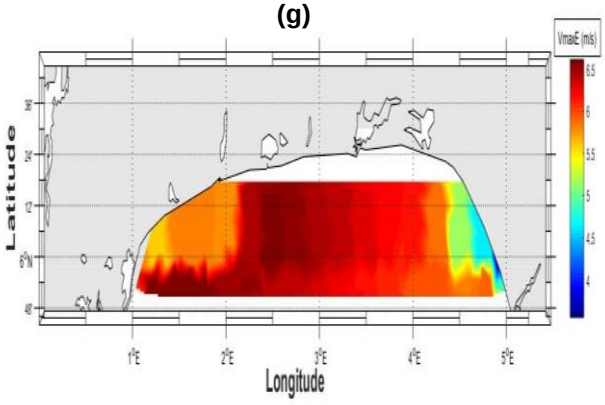
VmaxE (m/s)
6.5
6
5.5
5
4.5
4
Latitude
36
24
12
6°N
48
1°E
2°E
3°E
4°E
5°E
Longitude

(h)

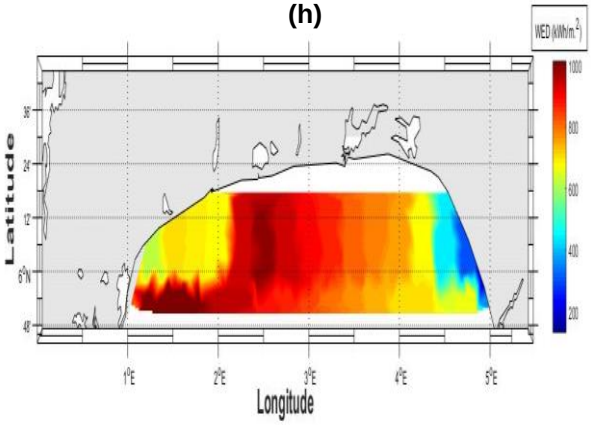
WED (kWh/m^2)
1000
800
600
400
200
Latitude
36
24
12
6°N
48
1°E
2°E
3°E
4°E
5°E
Longitude

Figure 9a-9h. Spatial Distribution of Wind Parameters in the Study Area.

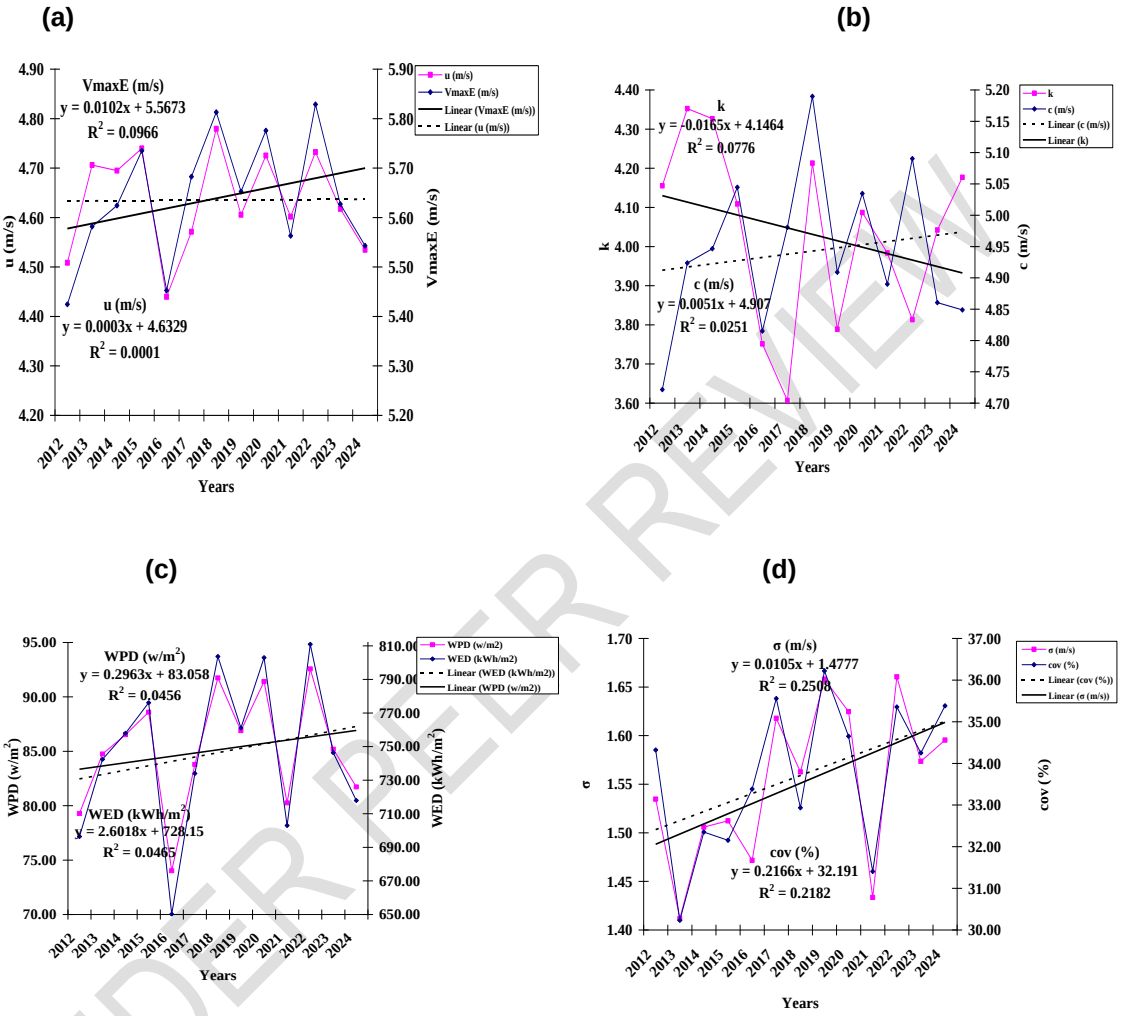

Figures 10 (a-d). Long Term Trends in the Yearly Averaged Values of the Wind Parameters.

5. CONCLUSION

This study assessed the spatio-temporal variability of wind power potential over Offshore Ondo State, Southwestern Nigeria, using Weibull parameters. It also examined the abundance of wave power in the area, focusing on regions with a seasonal average WVPD exceeding 6 kW/m and a coefficient of variation (COV) below 2.0. The research analyzed both the annual and monthly percentage frequencies of different wave power categories, along with their spatial distribution. The key findings from this study are summarized as follows:

(1) The study area generally showed poor wind characteristics. This is seen in higher values of the monthly and yearly averaged wind speeds with wind power densities throughout the study period.

(2) The computed annual average wind power (84.83w/m^2) characterizes the study area as being poor for wind power applications.
(3) The wind speed of 6.16 m/s was maximum in July, while a minimum value of 3.41 m/s occurred during November. The WPD fell within the range of 35.21 w/m^2 in November and 165.44 w/m^2 in July. The wind had the largest variation (36.23%) in November and the least (18.49%) in August, implying that the wind is most stable in November and least stable in August.
(4) The large region of higher wind power between 110 w/m^2 and 120 w/m^2 was centered in regions between Seme, Kpodji, and Ghana. These regions are marginal for connected wind power applications.
(5) For the periods that were studied, all the wind parameters, such as VmaxE, u10, c, WPD, WED, σ and COV, exhibited respective increasing trends of 0.0102 m/syr^{-1}, 0.0003 m/syr^{-1}, 0.0051 m/syr^{-1}, 0.29 w/m^2yr^{-1}, 2.6 kWh/m^2yr^{-1}, 0.01 m/syr^{-1} and 0.21 %yr^{-1}, except k, which showed a declining trend of -0.0165.
(6) The wave power is richest (> 6kW/m) in waters between longitudes 3.25^0 E - 3.75^0 E. This region is most ideal and recommended for the installation of wave energy converters for massive electrical energy generation in the study area. Additionally, a small location, precisely at 4.3^0 E and 6.1^0 N, closer to the Ondo State coastal waters, is also identified as a location with relatively rich wave power energy, with a wave power of around 5kW/m.
(7) The wave power in the category of 0≤wvpd≤5 is most centered (56%) in areas close to Ghana and Lome, and least centered (<46%) in the middle of the study area. For the 5≤wvpd≤10 category, the largest frequency (around 39.5%) occurred in waters south of Gbehoue. It is least concentrated (<37%) in waters around Aiyetoro, Awoye, Ghana, Lome and regions south of Vogan and Grand Popo. The percentage occurrence of the 10≤wvpd≤15 category is largest (~12%) in the mid-waters of the study area, and least (<8%) in regions around Aiyetoro, Awoye and the extreme west of the study locations. The remaining wave power categories have very little or no occurrence (< 3%) throughout the study region.
(8) Lastly, for the annual and monthly percentage cumulative frequency distribution of wave power, higher frequency of wave power values cluster around 0 to 10 kW/m across the study area. The wave power between 0 and 5 kW/m showed higher occurrences from October through March. The months of April through September showed higher frequencies for the 5-10 kW/m wave power category. The sea is more energetic and turbulent between June and August.

ETHICAL APPROVAL AND CONSENT TO PARTICIPATE

The data provided in this article is exempt from the requirement for ethical approval or participant consent.

COMPETING INTERESTS DISCLAIMER

Authors hereby declare that NO generative Artifitial Intelligence technologies such as Large Language Models (ChatGPT, COPILOT, etc.) and text-to-image generators have been used during the writing or editing of this manuscript.

REFERENCES

1. Tabibi, A. (2024). 2025 and Beyond: A Vision for the Ocean Energy Industry. https://green.org. www,Green.org.

2. Yang, X., Zhou, H., and Gao, J. (2024). Enhancing renewable energy productivity and energy efficiency of energy projects: How does cost of capital influence? Energy Strategy Reviews, 57, 101608. https://doi.org/10.1016/j.esr.2024.101608

3. Perez-Collazo, C., Greaves, D., and Iglesias, G. (2015). A review of combined wave and offshore wind energy. Renewable and Sustainable Energy Reviews, 42, 141–153. https://doi.org/10.1016/j.rser.2014.09.032

4. Korovushkin, V., Boichenko, S., Artyukhov, A., Cwik, K., Wróblewska, D., Jankowski, G. (2025). Modern Optimization Technologies in Hybrid Renewable Energy Systems: A Systematic Review of Research Gaps and Prospects for Decisions. Energies 2025, 18, 4727. https://doi.org/ 10.3390/en18174727

5. Giedraityte, A., Rimkevicius, S., Marciukaitis, M., Radziukynas, V., Bakas, R. (2025). Hybrid Renewable Energy Systems—A Review of Optimization Approaches and Future Challenges. Appl. Sci. 2025, 15, 1744. https://doi.org/ 10.3390/app15041744

6. African Development Bank Group, (2021). Assessing the Potential of Offshore Renewable Energy in Africa. 2021. African Natural Resources Center. https//www.afdb.org.

7. Upadhyaya, S. K., Rao, S., and Rao, M. (2024). Assessment of wind and wave energy potential along the Indian coast, Cogent Engineering, 11:1, 2316950, DOI: 10.1080/23311916.2024.2316950 To link to this article: https://doi.org/10.1080/23311916.2024.231695.

8. Rusu, E., and Onea, F. (2019). An assessment of the wind and wave power potential in the island environment,Energy,Volume 175,2019,Pages 830-846,ISSN 0360 5442,https://doi.org/10.1016/j.energy.2019.03.130.https://www.sciencedirect.com/science/article/pii/S0360544219305468

9. Gonzalez, N., Serna-Torre, P., Sánchez-Pérez, P. A., Davidson, R., Murray, B., Staadecker, M., Szinai, J., Wei, R., Kammen, D. M., Sunter, D. A., and Hidalgo-Gonzalez, P. (2024). Offshore wind and wave energy can reduce total installed capacity required in zero emissions grids. Nature Communications| (2024) 15:6826 https://doi.org/10.1038/s41467-024-50040-6.

10. Caires, S., Sterl, A., Bidlot, J. R., Graham, N., and Swail, V. (2004). Intercomparison of different wind-wave reanalyses, J. Clim., 17(10), 1893–1913.

11. Sterl, A. (2004). On the (in)homogeneity of reanalysis products, J. Clim.,17, 3866–3873.

12. Chang, E. K. M. (2007). Assessing the increasing trend in Northern Hemisphere winter storm track activity using surface ship observations and a statistical storm track model, J. Clim., 20, 5607–5628.

13. Cox, A. T., and Swail, V. R. (2001). A global wave hindcast over the period 1958–1997: Validation and climate assessment, J. Geophys. Res.,106(C2), 2313–2329.

14. Graham, N. E., and Diaz, H. F. (2001), Evidence for intensification of North Pacific winter cyclones since 1948, Bull. Am. Meteorol. Soc., 82(9),1869–1893.

15. Akdag, S. A., Güler, Ö. (2010). Evaluation of wind energy investment interest and electricity generation cost analysis for Turkey. Appl Energy 2010;87(8):2574-80.

16. Keyhani, A., Ghasemi-Varnamkhasti, M., Khanali, M., and Abbaszadeh, R. (2010). An assessment of wind energy potential as a power generation source in the capital of Iran, Tehran. Energy 2010;35(1):188–201.

17. Hamad, N., Millot, C., and Taupier-Letage, I. (2006). Scientia Marina 70, 457.

18. Bagiorgas, H. S., Mihalakakou, G., Rehman, S., and Al-Hadhrami, L. M. (2012). Wind power potential assessment for seven buoys data collection stations in Aegean Sea using Weibull distribution function. Journal of Renewable and Sustainable Energy 4, 013119 (2012). doi:10.1063/1.3688030

19. Zheng, C. W., Pan, J., Li, J. X. (2013). Assessing the China sea wind energy and wave energy resources from 1988 to 2009. Ocean Eng 2013; 65: 39-48. http://dx.doi.org/10.1016/j.oceaneng.2013.03.006

20. Jianli, R., Yuya, L., and Yingjie, Z. (2008). The implementation for the analysis system of ocean wave resources and the application of wave energy power generation. Journal of Zhejiang University of Technology (in Chinese) 2008; 36(2): 186-191.

21. Osinowo, A. A., Okogbue, E. C., Eresanya, E. O., and Akande, S. O. (2017). Evaluation of wind potential and its trends in the mid-Atlantic. Modeling Earth Systems and Environment (2017) 3:1199–1213 https://doi.org/10.1007/s40808-017-0399-4

22. Elliott, D., and Schwartz, M. (1993). Wind energy potential in the United States. Pacific Northwest Laboratory PNL-SA-23109, Richland, WA.

23. Enikanselu, P. A., Balogun, A. A., Ewetumo, T., Osinowo, A. A., Ogundare, M. O., Ashiru, O. R., Abe, J. S., Ifanegan, A. S., and Okunlola, B. A. (2025). Exploration of Wind-Wave Energy Potentials for Renewable Energy Development in Parts of Ondo Coastal and Offshore Locations, Southwestern Nigeria. Indian Journal of Energy and Energy Resources (IJEER) ISSN: 2583-1186 (Online), Volume-4 Issue-2, February 2025.

24. Osinowo, A. A., Balogun, I. A., and Eresanya, E. O. (2018). Assessment of wave energy resource in the mid-Atlantic based on 37- year numerical hindcast data. Modeling Earth Systems and Environment https://doi.org/10.1007/s40808-018-0484-3

25. Xydis, G., Koroneos, C., and Loizidou, M. (2009). Energy analysis in a wind speed prognostic model as a wind farm sitting selection tool: a case study in Southern Greece. Appl Energy 2009;86(11):2411-20.

26. Osinowo, A. A., and Popoola, S. O. (2024). Statistical evaluations of sea's state along the Nigerian coast. *Journal of Coastal Conservation*, 2024. *28*(1). DOI: https://doi.org/10.1007/s11852-023-01014-1

27. Olakunle, G. W., Osinowo, A. A., and Okunlola, B. A. (2021). Potentials for Wave Power Generation in Ayetoro, Ondo State, Nigeria. International Journal of Engineering Research-Online. 2021, vol 9 (4), https://www.researchgate.net/publication/373797793. Potentials for wave power generation in Ayetoro, Ondo State, Nigeria.

28. Osinowo, A. A., and Popoola, S. O. (2021). Long-term spatio-temporal trends in extreme wave events in the Niger delta coastlines. *Continental Shelf Research*,2021, *224*, 104471. DOI: https://doi.org/10.1016/j.csr.2021.104471

29. Olakunle, G. W., Salami, M., and Osinowo, A. A. (2021). Assessment of Sea Incursion and Flood Susceptibility Factors In Ayetoro Fishing Community of Ondo State, Nigeria. Journal of Advanced Studies in Agricultural, Biological and Environmental Sciences (JABE) 2021, Vol.8. (2) http://jabe.in/8.2.21/1-13%20OLAKUNLE,%20G.%20W.pdf

30. Ishaku, H. T., and Rafee-Majid, M. (2010). X-Raying Rainfall Pattern and Variability in North-eastern Nigeria: Impacts on Access to Water Supply. J. Water Resource and Protection, 2:952-959. 2010. DOI: http://doi.org/10.4236/jwarp.2010.211113.

31. Omosuyi, G. O., Ojo, J. S., and Olorunfemi, M. O. (2008). Geoelectric Sounding to Delineate Shallow Aquifers in the Coastal Plain Sands of Okitipupa Area, Southwestern Nigeria. Pacific Journal of Science and Technology. 9(2). 2008. 562-577. http://www.akamaiuniversity.us/PJST.htm

32. Asiwaju-Bello, Y. A. and Owoseni, J. O. (2023). Hydrogeology of the coastal region of Ondo State, Nigeria. Engineering Research Journal, 3(5), 2023, 37-50.ISSN: 2782-8212. https://www.ijaar.org/erj.

33. Wilks, D. S. (1995). Statistical Methods in the Atmospheric Sciences: An Introduction. Academic Press, San Diego, Calif, USA.

34. Ohunakin, O., Adaramola, M., and Oyewola, O. (2011). Wind energy evaluation for electricity generation using WECS in seven selected locations in Nigeria. Appl Energy 88(9) 3197–206.

35. Gökçek, M., Bayülken, A., Bekdemir, S. (2007). Investigation of wind characteristics and wind energy potential in Kirklareli, Turkey. Renewable Energy 32(10) 1739–52.

36. Fyrippis, I., Axaopoulos, P. J., and Panayiotou, G. (2010). Wind energy potential assessment in Naxos Island, Greece. Appl Energy, 87(2) 577–86.

37. Justus, C., Hargraves, W., Mikhail, A., and Graber, D. (1978). Methods for estimating wind speed frequency distributions. J Appl Meteorol 17(3) 350–3.

38. Akdag, S. A., Dinler A. (2009). A new method to estimate Weibull parameters for wind energy applications. Energy Convers Manage 50(7) 1761–6.

39. Stevens, M., Smulders, P. (1979). The estimation of the parameters of the Weibull wind speed distribution for wind energy utilization purposes. Wind Eng 3 132–45.

40. Rinne, H. (2010). The Weibull distribution: a handbook. CRC Press

41. Khan, J. K., Ahmed, F., Uddin, Z., Iqbal, S. T., Saif, U. J., Siddiqui, A. A., and Aijaz, A. (2015). Determination of Weibull Parameter by four Numerical Methods and Prediction of Wind Speed in Jiwani (Balochistan). J Basic Appl Sci 11, 62-68. http://dx.doi.org/10.6000/1927-5129.2015.11.08

42. Saleh, H., Abou El-Azm Aly, A., and Abdel-Hady, S. (2012). Assessment of different methods used to estimate Weibull distribution parameters for wind speed in Zafarana wind farm, Suez Gulf, Egypt. Energy 44(1) 710–9.

43. Manwell, J. F., McGowan, J. G., and Rogers, A. L. (2002). Wind energy explained: theory, design and application, Amherst (USA). John Wiley & Sons.

44. Sathyajith, M. (2006). Wind energy: fundamentals, resource analysis and economics, Springer.

45. Tchinda, R., Kendjio, J., Kaptouom, E., and Njomo, D. (2000). Estimation of mean wind energy available in far north Cameroon. Energy Convers Manage, 41 (17) 1917–29.

46. Jamil, M., Parsa, S., and Majidi, M. (1995). Wind power statistics and evaluation of wind energy density. Renew Energ, 6 (5-6) 623-8.

47. Ahmed, A. S. (2012). Investigation potential wind power generation in South Egypt. J Renew Sustain Energy, Rev16 1528–36.

48. Cornett, A. M. (2008). A global wave energy resource assessment. In: Proceedings of the eighteenth international offshore and polar engineering conference (ISOPE), International Society of Offshore and Polar Engineers, Paper No. ISOPE-2008-579. Vancouver, July 6–11, 2008.

49. Iglesias, G., and Carballo, R. (2011). Choosing the site for the first wave farm in a region: A case study in the Galician Southwest (Spain). Energy 36(9), 5525–5531, 2011.

50. Vosough, A. (2011). Wave power. Int. J. Multidiscip. Sci. Eng. 2(7), 60–63, 2011.

51. Zheng,C. W., Zhou, L., Jia, B. K., Pan, J. L., and Li, X. (2014). Wave characteristic analysis and wave energy resource evaluation in the China Sea. Journal of Renewable and Sustainable Energy 6, 043101; http://dx.doi.org/10.1063/1.4885842, 2014.

ABBREVIATIONS

cc: Correlation coefficient
WED: Wind Energy Density

WPD: Wind Power Density

COV: Coefficient of Variation

Vmax.E: Wind Speed carrying Maximum Energy
K: Weibull shape parameter
C: Scale parameter
WVPD: Wave Power Density